ferred and expressed in synthetic systems in a way similar to nature. An interesting mechanism is suggested by which chirality is amplified to give supramolecular (helical) chirality, namely through the following processes: The S-chiral centers in the tails induce a clockwise orientation of the molecular disks which, aided by strong π-π stacking, leads to the formation of fibers with right-handed helicity. Side-on aggregation of the fibers subsequently yields supercoiled structures with left-handed helicity. Such a control over chirality may be valuable in designing new materials for optoelectronic applications. The present chiral fibers are attractive candidates for use as nonlinear optical materials and as components in sensor devices, for example, for the detection of alkali metal ions.

References and Notes

1. D. R. Eyre, *Science* **207**, 1315 (1980).
2. A. D. McLachlan, *Annu. Rev. Biophys. Bioeng.* **13**, 167 (1984).
3. R. E. Franklin, *Nature* **175**, 379 (1955); ______ and A. Klug, *Acta Crystallogr.* **8**, 777 (1955).
4. D. Goldhaber-Gordon *et al.*, *Proc. IEEE* **85**, 521 (1997).
5. R. S. Lokey and B. L. Iverson, *Nature* **375**, 303 (1995); J. C. Nelson *et al.*, *Science* **277**, 1793 (1997); G. S. Hanan *et al.*, *J. Chem. Soc. Chem. Commun.* (1995), p. 765; D. M. Bassani *et al.*, *Angew. Chem. Int. Ed. Engl.* **36**, 1845 (1997); P. Mariani, F. Ciuchi, L. Saturni, *Biophys. J.* **74**, 430 (1998); N. Kimizuka *et al.*, *J. Chem. Soc. Chem. Commun.*, 2103 (1995).
6. C. C. Leznoff and A. B. P. Lever, Eds., *Phthalocyanines, Properties and Applications* (VCH, New York, 1989–1996), vols. 1 to 4.
7. T. M. Fyles and W. F. van Straaten-Nijenhuis, in *Comprehensive Supramolecular Chemistry*, J. L. Atwood, *et al.*, Eds. (Elsevier Science, Oxford, 1996), vol. 10, chap. 3.
8. J. F. van der Pol *et al.*, *Liq. Cryst.* **6**, 577 (1989).
9. H. Engelkamp, S. Middelbeek, R. J. M. Nolte, in preparation.
10. N. Harada and K. Nakanishi, *Circular Dichroic Spectroscopy—Exciton Coupling in Organic Chemistry* (Oxford Univ. Press, Oxford, 1983), pp. 6–9.
11. W. Caseri, T. Sauer, G. Wegner, *Makromol. Chem. Rapid Commun.* **9**, 651 (1988).
12. H. Engelkamp, C. F. van Nostrum, S. J. Picken, R. J. M. Nolte, *Chem. Commun.*, 979 (1998).
13. C. J. Pedersen, *J. Am. Chem. Soc.* **89**, 7017 (1967).
14. O. E. Sielcken *et al.*, *ibid.* **109**, 4261 (1987).
15. C. F. van Nostrum *et al.*, *ibid.* **117**, 9957 (1995).
16. Persistence of Vision(tm) Ray-Tracer [POV-Ray(tm)] version 3.02, Persistence of Vision Development Team (tm).

17. Funded by the Netherlands Foundation for Chemical Research with financial aid from the Netherlands Organization for Scientific Research.

6 January 1999; accepted 22 March 1999

Pressure-Induced Solid Carbonates from Molecular CO_2 by Computer Simulation

S. Serra,[1,2] C. Cavazzoni,[1,2] G. L. Chiarotti,[1,2]* S. Scandolo,[1,2] E. Tosatti[1,2,3]

A combination of ab initio molecular dynamic simulations and fully relaxed total energy calculations is used to predict that molecular CO_2 should transform to nonmolecular carbonate phases based on CO_4 tetrahedra at pressures in the range of 35 to 60 gigapascals. The simulation suggests a variety of competing phases, with a more facile transformation of the molecular phase at high temperatures. Thermodynamically, the most stable carbonate phase at high pressure is predicted to be isostructural to SiO_2 α-quartz (low quartz). A class of carbonates, involving special arrangements of CO_4 tetrahedra, is found to be more stable than all the other silica-like polymorphs.

Carbon and silicon, although isoelectronic and close in their solid state behavior in several ways, differ markedly when fully oxidized. In carbon, the stability of CO_2 is so overwhelming that no other nonmolecular solid state forms are known. In silicon, by contrast, the phase diagram is dominated by solid state silicates, because the stability of molecular SiO_2 is poorer than that of CO_2. The wide range of electrical and optical applications of SiO_2 quartz (such as piezoelectricity and optical nonlinearities) derive from its noncentrosymmetric crystal structure. If CO_2 could be synthesized in a covalently bonded noncentrosymmetric structure, these properties would be complemented by the higher mechanical strength of the less deformable C–O covalent bond with respect to the Si–O one. Here we present theoretical calculations and simulations, indicating that ultrahigh pressures should reduce the stability of molecular CO_2 in favor of quartzlike nonmolecular solid state carbonates.

The crystalline structure of solid molecular CO_2 is characterized by the large quadrupole moment of the linear CO_2 molecule, which dominates the long-range intermolecular interactions (*1, 2*). The cubic Pa3 structure (α-CO_2) prevails at room temperature for pressures lower than 11 GPa (*3–5*). With increasing pressure above 11 GPa, a second quadrupolar molecular phase, an orthorhombic *Cmca* (β-CO_2) (Fig. 1A), prevails (*5, 6*). This *Cmca* molecular phase persists to at least 50 GPa (*7, 8*), but no further knowledge is presently available of additional phase transition, before eventual pressure-induced chemical decomposition (*9*).

We have explored this unknown pressure region by constant pressure molecular dynamics (MD) simulations based on the variable-cell method (*10*). The first-principles density functional nature of the method and the variable cell dynamics are effective for simulating pressure-induced solid-solid phase transformations in a variety of systems (*11*), including the characterization of the pressure-induced polymerization of carbon monoxide (*12*). The density functional scheme used is based on the Becke-Lee-Yang-Parr generalized gradient-corrected local density approximation (LDA/GGA) (*13*), and nonlocal (*14*) pseudopotentials for ion cores (*15*). Wavefunctions for MD simulations were expanded in plane waves with an energy cutoff of 80 Ry and Γ point sampling of the Brillouin zone (BZ). Final electronic and structural refinements were obtained by fully converged k-point sampled calculations and 100 Ry cutoff.

The validity of the computational scheme was initially checked by comparing our optimized β-CO_2 molecular lattice structure with the x-ray data at 12 GPa (*5*). Our calculated structures are consistent with the experimentally derived structure, especially in the fully converged k-points calculations [256 k-points in the full BZ], where errors in the lattice constants are less than 0.3%. Moreover, the tilt angle of the molecules relative to the *c* axis, usually difficult to reproduce because of its weak energy dependence, is calculated to be 52.5°, consistent with the experimental value of 52°. We also confirm, as already found by Gygi (*6*), that molecules lie in the plane identified by the *c* axis and the shorter axis of the basal plane. These results show that the LDA/GGA description of solid molecular CO_2 can be used to explore the high-pressure phase diagram of solid CO_2.

The first MD simulation was started with an orthorhombic simulation box containing 16 CO_2 molecules initially in the β-CO_2 phase at 12 GPa, with a time step of 0.3 fs. The temperature was equilibrated (*16*) at 300 K for 3 ps, during which the β-CO_2 structure remained stable. Pressure was then increased

---

[1] International School for Advanced Studies (SISSA), Via Beirut 4, I-34014 Trieste, Italy. [2] Istituto Nazionale per la Fisica della Materia (INFM), Via Beirut 4, I-34014 Trieste, Italy. [3] International Center for Theoretical Physics (ICTP), Post Office Box 586, I-34014 Trieste, Italy.

*To whom correspondence should be addressed. E-mail: guido@sissa.it

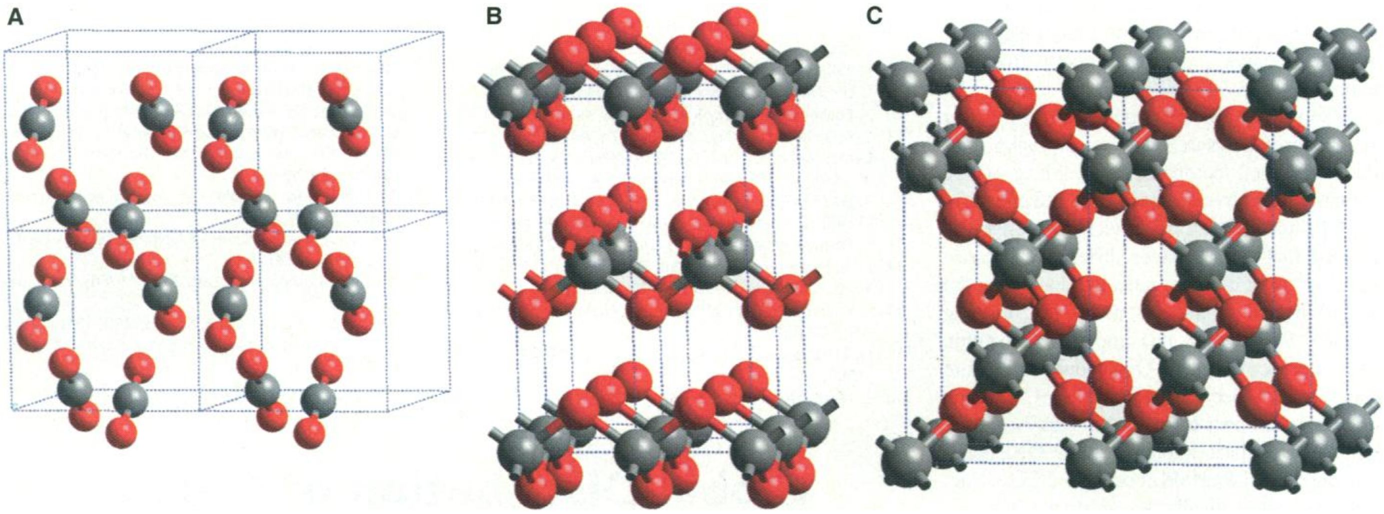

Fig. 1. (**A**) View of four conventional unit cells of the β-CO_2 phase. (**B**) Lateral view of the layered-CO_2 phase. (**C**) Crystal structure of m-chalcopyrite. Carbon atoms are colored gray and oxygen atoms are colored red.

without temperature control at a rate of 25 GPa/ps for 6 ps. At 130 GPa and 1000 K a reconstructive transition spontaneously occurred, with a sizable decrease in volume ($\Delta V/V \sim 9\%$). The resulting structure was a solid consisting of carbon-centered oxygen tetrahedra, similar to Si-centered tetrahedra in silica, arranged in a two-dimensional (2D) tetragonal layered structure (henceforth named layered-CO_2), of space group *P*42/*nmc* and two CO_2 units per cell (Fig. 1B). The known structure closest to that of layered-CO_2 is that of red tetrahedral HgI_2, where however the metal site is only approximately tetrahedrally coordinated. The outcome of this first simulation run suggests the existence of well-defined CO_4 tetrahedra-based solids.

We carried out two subsequent simulation runs, with 24 and 48 CO_2 molecules, at 2000 K. In these higher temperature simulations the β-CO_2 structure transformed into a silica-like 3D amorphous solid. This 3D amorphous phase is characterized, as the 2D layered CO_2, by having carbon atoms at the fourfold center of oxygen tetrahedra, and oxygen atoms twofold coordinated, in a bridge position between two carbons. Amorphization could possibly be an artifact of the short simulation times and fast compression rates. However, the 3D local coordination of the CO_4 tetrahedra indicates that 3D ordered structures like those observed in SiO_2 may be energetically competitive with the layered 2D carbonate found in the first low-*T* simulation. A 3D analog of the layered carbonate can be obtained by removing one of the metal ions of $CuFeS_2$ (chalcopyrite), replacing the remaining metal ion with carbon, and sulfur with oxygen (*17*). This leads to a 3D CO_2 crystal structure (Fig. 1C), which we call m-chalcopyrite, that differs from the 2D layered carbonate starting from the fifth nearest neighbor shell. Indeed, the 48-CO_2 simulation reveals that some of the tetrahedra are organized as in the m-chalcopyrite crystal structure described above.

To identify the most stable structure among those suggested by the simulations, we carried out separate, well-converged, fully relaxed refinement calculations for a selected set of reasonable crystalline candidates for the high-pressure phases of CO_2, namely, α-quartz, cristobalite, coesite, stishovite, m-chalcopyrite, layered-CO_2, and, of course, the initial molecular β-CO_2 phase. All the nonmolecular structures are carbonates with tetrahedral carbon coordination, apart from stishovite, where the local carbon coordination is six. For α-quartz, coesite, stishovite, β-CO_2, and layered-CO_2 the total energy calculations were carried out for a set of volumes and enthalpies fitted by a Birch-Murnaghan equation of state. For cristobalite and m-chalcopyrite, because of the complexity of their unit cells, enthalpy was evaluated only at a single pressure.

The molecular β-CO_2 phase is correctly found to be stable for pressures lower than 35 GPa (Fig. 2), whereas the α-quartz phase is predicted to be stable at all pressures exceeding 35 GPa and, barring other structures not considered in this work, up to the highest calculated pressure (500 GPa). As evident from Fig. 2, the enthalpy of the amorphous solid found in the high-temperature simulation is only slightly higher than that of crystalline α-quartz, and similar to that of other tetrahedral crystalline structures. The angular distribution of the C–O–C bending angles, a distinctive feature of different crystal structures, shows that the amorphous solid obtained in the simulation is more similar to m-chalcopyrite and to α-quartz than to any other structure considered. The appearance of an amorphous quartzlike structure in high-temperature MD simulations suggests that a considerable energy barrier has to be overcome to transform molecular CO_2 to α-quartz CO_2. Such an energy barrier may be responsible for the inability of α-quartz to appear in room temperature experiments up to 50 GPa. This suggests that heating to high temperature (around 2000 K) may be a crucial factor when trying to synthesize α-quartz near the thermodynamical transition pressure. This is not the case for layered-CO_2, which we found in the first low-temperature simulation. The absence of significant energy barriers, together with its relative energetic stability (Fig. 2), suggests that the layered-CO_2 might indeed be obtained as a metastable state under appropriate experimental conditions (for example, fast and cold compression), at pressures larger than the thermodynamical β-CO_2→layered-CO_2 transition pressure, which we find to be 60 GPa (Fig. 2). This may also be the case for m-chalcopyrite, and in fact for a whole (infinite) class of structures, whose common ingredient is that all corner-shared CO_4 tetrahedra have the same spatial orientation, leading to a single value of 109° for the C–O–C bending angles. On the other hand, the stishovite structure, where carbon is sixfold coordinated, is largely disfavored over all fourfold coordinated structures and over the full dissociation into C (diamond) +

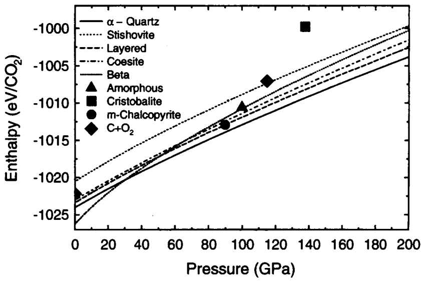

Fig. 2. Enthalpy versus pressure for the solid phases of CO_2.

O_2 (molecular). It is thus possible that CO_2 will finally dissociate into its constituent elements, at multimegabar pressures, directly from the α-quartz phase.

The stability of the α-quartz structure over such a large pressure range is surprising, particularly when compared with SiO_2, where α-quartz is observed to transform into coesite at 2.1 GPa and then into stishovite at 7.6 GPa. We suggest that CO_2 behaves differently because the C sp^3 hybrid is energetically closer than the Si sp^3 hybrid to the p state of the bridging oxygen. Structurally, this implies stabilization of a more covalent C–O–C bond and, more specifically, a decrease of the C–O–C bending angle with respect to Si–O–Si. This is consistent with our observation that the C–O–C bending angle in all fourfold coordinated CO_2 structures is systematically lower than the corresponding values for SiO_2 (for α-quartz at zero pressure, we find for CO_2 a bending angle of 137°, compared with a value of 144° for SiO_2). Preference for low C–O–C bending angles may then explain why CO_2 cristobalite, where all bending angles are fixed by symmetry to 180°, and coesite, where the same is true for one of the bending angles, are energetically disfavored (Fig. 2). This may also be the rationale for the appearance of the layered-CO_2 structure, and m-chalcopyrite, where the bending angles are found to be about 109° at all pressures.

If α-quartz CO_2 could be quenched to zero pressure, we predict that its lattice parameters would be $a = 4.13$ Å and $c = 4.58$ Å, its density 3.28 g/cm^3, and its bulk modulus 183 GPa. It would be insulating, with an energy gap that we estimate to be around 10 eV (*18*). We also calculated the piezoelectric strain coefficient (*19*) of α-quartz CO_2 at zero pressure, and found it to be 1.0 pC/N, about 40% that of SiO_2, possibly as a result of the lower ionicity of α-quartz CO_2. Finally, we give an estimate of the relative value of the second harmonic intensity I_{SH} of α-quartz CO_2 with respect to that of α-quartz SiO_2. I_{SH} is proportional (*20*) to the square of the second-order susceptibility $\chi^{(2)}$ that can be estimated with Miller's rule (*21*), and the fact that first-order susceptibility roughly scales linearly with electron density and with the inverse square of the energy gap. I_{SH} of α-quartz CO_2 estimated in this way is about 50 times larger than that of α-quartz SiO_2.

Note added in proof: Recently, Iota *et al.* (*22*) have shown that, in agreement with our findings, quartzlike CO_2 can in fact be synthesized above 40 GPa and 1800 K.

References and Notes

1. C. A. English and J. A. Venables, *Proc. R. Soc. London Ser. A.* **340**, 57 (1974).
2. B. Kuchta and R. D. Etters, *Phys. Rev. B* **38**, 6265 (1988).
3. D. A. Dows and V. Schettino, *J. Chem. Phys.* **58**, 5009 (1973).
4. H. Olijnyk *et al.*, *ibid.* **88**, 4204 (1988).
5. K. Aoki *et al.*, *Science* **263**, 356 (1994).
6. F. Gygi, *Comput. Mater. Sci.* **10**, 63 (1998).
7. R. Lu and A. M. Hofmeister, *Phys. Rev. B* **52**, 3985 (1995).
8. H. Olijnyk and A. P. Jephcoat, *ibid.* **57**, 879 (1998).
9. L. Liu, *Earth Planet. Sci. Lett.* **71**, 104 (1984).
10. P. Focher *et al.*, *Europhys. Lett.* **36**, 345 (1994).
11. S. Scandolo *et al.*, *Phys. Rev. Lett.* **74**, 4015 (1995); M. Bernasconi *et al.*, *ibid.* **78**, 2008 (1997); J. Kohanoff *et al.*, *ibid.*, p. 2783; F. Ancilotto *et al.*, *Science* **275**, 1288 (1997); S. Serra *et al.*, *Phys. Rev. Lett.* **80**, 5160 (1998); C. Cavazzoni *et al.*, *Science* **283**, 44 (1999).
12. S. Bernard *et al.*, *Phys. Rev. Lett.* **81**, 2092 (1998).
13. A. D. Becke, *Phys. Rev. A* **38**, 3098 (1988); C. Lee, W. Yang, R. G. Parr, *ibid. B* **37**, 785 (1988).
14. L. Kleinman and D. M. Bylander, *Phys. Rev. Lett.* **48**, 1425 (1982).
15. N. Trouiller and J. L. Martins, *Phys. Rev. B* **43**, 1993 (1991).
16. S. Nosé, *Mol. Phys.* **52**, 255 (1984).
17. In this structure carbon is fourfold coordinated to oxygen, oxygen twofold coordinated to carbon, and the C–O–C bending angle is 109°.
18. The LDA is known to underestimate band gaps. We calculate a LDA/GGA gap of 6.5 eV for α-quartz CO_2. In α-quartz SiO_2 the LDA/GGA band gap is also 6.5 eV, compared with an experimental value of about 10 eV. Here we assume that the same correction applies to CO_2.
19. D. Vanderbilt, available at xxx.lanl.gov/abs/cond-mat/9903137.
20. Y. R. Shen, *The Principles of Nonlinear Optics* (Wiley, New York, 1984).
21. R. C. Miller, *Appl. Phys. Lett.* **5**, 17 (1964); Y. R. Shen, in (*20*), p. 37.
22. V. Iota, C. S. Yoo, H. Cynn, *Science* **283**, 1510 (1999).

23. We acknowledge partial support from INFM and MURST.

21 December 1998; accepted 18 March 1999

Global Distribution of Crustal Magnetization Discovered by the Mars Global Surveyor MAG/ER Experiment

M. H. Acuña,[1] J. E. P. Connerney,[1] N. F. Ness,[2] R. P. Lin,[3] D. Mitchell,[3] C. W. Carlson,[3] J. McFadden,[3] K. A. Anderson,[3] H. Rème,[4] C. Mazelle,[4] D. Vignes,[4] P. Wasilewski,[1] P. Cloutier[5]

Vector magnetic field observations of the martian crust were acquired by the Mars Global Surveyor (MGS) magnetic field experiment/electron reflectometer (MAG/ER) during the aerobraking and science phasing orbits, at altitudes between ~100 and 200 kilometers. Magnetic field sources of multiple scales, strength, and geometry were observed. There is a correlation between the location of the sources and the ancient cratered terrain of the martian highlands. The absence of crustal magnetism near large impact basins such as Hellas and Argyre implies cessation of internal dynamo action during the early Naochian epoch (~4 billion years ago). Sources with equivalent magnetic moments as large as 1.3 × 10^{17} ampere-meter^2 in the Terra Sirenum region contribute to the development of an asymmetrical, time-variable obstacle to solar wind flow around Mars.

The primary science goals of the MAG/ER investigation are the detection and characterization of the magnetic field of the planet and the study of its interaction with the solar wind. Vector measurements of the ambient magnetic field are acquired by a twin fluxgate magnetometer system. An electron reflection analyzer is used to remotely sense magnetic fields of planetary origin at the top of the martian atmosphere and to provide information about the local electron distribution function (*1*, *2*). Measurements made early in the mission established unambiguously that Mars does not currently possess a significant global magnetic field, with an estimated upper limit for a Mars dipole moment of ~2 × 10^{18} A-m^2.

At the same time the detection of strong, small-scale crustal magnetic sources associated with the ancient, heavily cratered terrain revealed that Mars must have had an internal active dynamo in its past, which is now extinct (*1*).

The first part of the aerobraking phase of MGS (AB1) was carried out between September and November 1997 and was followed by aerobraking hiatus orbits (AHO) and science phasing orbits SPO1 and SPO2 from March to July 1998. The latter were designed to allow the heliocentric motion of Mars to bring the spacecraft orbit plane into the desired alignment with the Mars-sun direction before initiating the second aerobraking phase AB2 and "pop-up" maneuver which would raise periapsis to achieve the final mapping orbit. These recently com-

---

[1] NASA Goddard Space Flight Center, Greenbelt, MD 20771, USA. [2] Bartol Research Institute, University of Delaware, Newark, DE 19716, USA. [3] Space Sciences Laboratory, University of California, Berkeley, CA 94720, USA. [4] Centre d'Etude Spatiale des Rayonnements, 31028 Toulouse Cedex 4, France. [5] Department of Space Physics and Astronomy, Rice University, Houston, TX, 77005, USA.